Toroidal quantum states in molecular spin-frustrated triangular nanomagnets with weak spin-orbit coupling: Applications to molecular spintronics

Jared M. Crabtree and Alessandro Soncini*
School of Chemistry, University of Melbourne, Parkville, Victoria 3010, Australia

(Received 13 May 2018; published 14 September 2018)

We theoretically investigate the ground-state spin texture and spin transport properties of triangular rings with on-site spins $S_q = \frac{1}{2}$ ($q = 1$–3). In the limit of strong antiferromagnetic exchange coupling and weak spin-orbit coupling, we find it is possible to prepare a noncollinear degenerate ground state with a *zero magnetic moment* and a *nonzero toroidal moment* $\boldsymbol{\tau} = g\mu_B \sum_q \mathbf{r}_q \times \mathbf{S}_q$, aligned along the C_3-symmetry axis. These pure toroidal states can be prepared: (i) within the fourfold degenerate spin-frustrated ground state even without any spin-orbit coupling; (ii) within the ground Kramers doublet resulting from weak spin-orbit splitting of the fourfold degenerate frustrated manifold via Dzyaloshinskii-Moriya antiferromagnetic exchange coupling. We also investigate the relationship between toroidal states and chiral spin states, characterized by the eigenvalues of the scalar spin chirality operator $\hat{\chi} = \frac{4}{\sqrt{3}}\hat{\mathbf{S}}_1 \cdot \hat{\mathbf{S}}_2 \times \hat{\mathbf{S}}_3$, and find that, since $[\hat{\boldsymbol{\tau}}, \hat{\chi}] \neq 0$, it is not possible to prepare states that are both toroidal and chiral simultaneously. Finally, by setting up a quantum transport model in the Coulomb blockade regime, we find that a spin current injected through a spin-polarized source electrode into the triangle is partially reversed upon scattering with the molecular toroidal states. This spin-switching effect is, in fact, a signature of molecular spin-transfer torque, which can be harnessed to modify the nonequilibrium populations of the $+\tau$- and $-\tau$-toroidal states, thus, to induce a net toroidal magnetization in the device using a spin current.

DOI: 10.1103/PhysRevB.98.094417

I. INTRODUCTION

A toroidal moment, also known as an anapole moment [1], is generated by a vortex arrangement of magnetic moments, which can have their origin in atomic spins and orbital currents [2]. It can be defined as the antisymmetric part of a general magnetic quadrupole moment, which is odd under both time-reversal and space inversion transformations [3,4], and hence, in an ordered phase [2], it can give rise to a linear magnetoelectric effect [5].

In molecules, pure toroidal moments were first identified in 2008 when molecular quantum states having a large nonzero toroidal moment and a zero magnetic moment were predicted in strongly anisotropic molecular spin rings [6] and identified [7,8] in a Dy_3 triangle [9]. These systems featured a nonmagnetic degenerate ground state, originating from the interplay between strong on-site magnetic anisotropy featuring in-plane tangential easy axes (thus requiring strong spin-orbit coupled systems) and weak antiferromagnetic exchange coupling [6]. Under such assumptions, the degenerate but nonmagnetic ground state of the polynuclear ring-shaped complex displays a nonzero toroidal moment defined as the expectation value of the following operator:

$$\hat{\boldsymbol{\tau}} = g\mu_B \sum_{q=1}^{N} \hat{\mathbf{r}}_q \times \hat{\mathbf{S}}_q, \tag{1}$$

where g is the Landé g factor, μ_B is the Bohr magneton, N is the number of spin centers in the ring, $\hat{\mathbf{S}}_q$ is the spin operator of center q, and $\hat{\mathbf{r}}_q$ is the position vector operator of center q relative to the middle of the ring.

The discovery of a toroidal moment in the Dy_3 triangular molecule [7,8] sparked a number of investigations of its magnetoelectric and molecular spintronics properties [10–12] as well as the identification and possible enhancement of toroidal ground states in many other Dy^{3+}-based polynuclear complexes [13–15] and in chiral heterometallic Cu^{2+}/Dy^{3+} polymers [16]. These systems were dubbed single-molecule toroics [11] and are expected to be promising candidates to develop molecular spintronics devices and molecular toroidal qubit devices. (See the recent review by Ungur *et al.* [17] and references therein.)

In order to harness toroidal states in spintronics devices or to develop toroidal molecular qubits for quantum computation, it is necessary to control the dynamics of these states via external fields. It should be noted however that direct manipulation of molecular quantum toroidal states using magnetic fields would require control on the molecular scale of magnetic-field gradients with a nonzero curl component $\boldsymbol{\nabla} \times \mathbf{B}$ [3,4]. As experimental control of field inhomogeneities on the molecular scale is not easily achievable, the use instead of electric currents [11,12] or spin currents [10] to control the dynamics of toroidal states has been proposed as an alternative route to toroidal state manipulation, expected to be within reach in the fast evolving field of experimental molecular spintronics [18–25]. In particular, ground states that are characterized by a toroidal moment have been shown to work as spin switches in a molecular spintronics circuit [10]. Also, the underlying spin-transfer torque leading to the spin-switching effect can be harnessed to initialize the system's quantum state in one particular toroidal moment $+\tau$ or $-\tau$ perpendicular to the molecular plane [10].

All efforts described so far aimed at the characterization of molecular toroidal moments and the manipulation of their

*asoncini@unimelb.edu.au

dynamics via electric or spin currents have been directed towards systems in the strong spin-orbit coupling and weak exchange-coupling limit. In particular, all these efforts have concerned strongly spin-orbit coupled systems [17]. A different route to achieve noncollinear canted spin moments in *weakly* spin-orbit coupled molecules consists of harnessing spin-frustrated states in strongly antiferromagnetically exchange-coupled spin rings, such as Cu_3 or V_3 [3,26–31]. In particular, it has been shown that spin triangles with local spin-$\frac{1}{2}$ metal centers can be harnessed to achieve new chiral quantum numbers where the scalar spin chirality operator is defined as $\hat{\chi} = \frac{4}{\sqrt{3}}\hat{\mathbf{S}}_1 \cdot \hat{\mathbf{S}}_2 \times \hat{\mathbf{S}}_3$ [3,27,28]. Furthermore, it was shown in 2008 that through linear superpositions of states with opposite spin chiralities, nonmagnetic toroidal states could be realized [3]. Here, we characterize the symmetry properties and spin textures of these states and propose their application in a molecular spintronics device.

A subsequent proposal to achieve a toroidal moment in a frustrated spin triangle was put forth in 2009 whereby a toroidal moment appeared in directions perpendicular to a V_3 triangle's ideal C_3-symmetry axis due to vibronic coupling effects [32]. In that case, the toroidal moment was mainly a measure of the noncollinear spin texture of the resulting spin states and coexisted with a perpendicular magnetic moment in the resulting spin states [32].

Since the toroidal moment is the antisymmetric part of a general magnetic quadrupole operator, it follows that the toroidal moment is origin dependent in systems with a nonzero magnetic moment [3,4]. In such systems, it is not possible to provide an origin-independent definition of a toroidal spin state [3,4]. Conversely, in systems with zero magnetic moments, the toroidal moment is origin independent as it is the first nonzero magnetic multipole moment. Hence, only systems with zero magnetic moments but nonzero toroidal moments can be unambiguously characterized by a pure toroidal spin texture.

In this paper we theoretically show that collective spin states characterized by a pure toroidal moment, hence a zero magnetic moment, can indeed be achieved in weakly spin-orbit coupled and strongly antiferromagnetically exchange-coupled spin-frustrated triangular rings. Furthermore, we present a theoretical and computational quantum transport model in the Coulomb blockade regime showing how noncollinear toroidal spin states in spin-frustrated triangles can be harnessed in spintronics circuits to reverse the sign of an injected spin current (spin-switching effect). Our model also shows that such a spin-switching effect is, in fact, based on a molecular spin-transfer torque effect whereby the injected spin current induces a nonzero toroidal polarization in the spin-frustrated triangular device. In other words, our results show that a spin current can be harnessed to electrically manipulate pure toroidal spin states within the weak spin-orbit coupling limit.

II. PURE TOROIDAL STATES IN SPIN-FRUSTRATED TRIANGLES

We define our molecular wheel as three spin-$\frac{1}{2}$ atomic centers, arranged as an equilateral triangle lying on the XY plane with its center at the origin. The full spin Hamiltonian reads [27]

$$\hat{H}_0 = -J_{\rm ex}\sum_{q=1}^{3}\hat{\mathbf{S}}_q \cdot \hat{\mathbf{S}}_{q+1} + D_{\rm DM}\sum_{q=1}^{3}(\hat{\mathbf{S}}_q \times \hat{\mathbf{S}}_{q+1})_Z, \qquad (2)$$

with contributions from Heisenberg exchange coupling and the symmetry-allowed component of the asymmetric Dzyaloshinskii-Moriya (DM) exchange interaction produced by spin-orbit coupling [27]. Assuming an antiferromagnetic exchange-coupling constant (i.e., $J_{\rm ex} < 0$), the ground exchange manifold will be spin frustrated, displaying two degenerate $S_{\rm tot} = \frac{1}{2}$ Kramers doublets. These ground doublets are separated from the $S_{\rm tot} = \frac{3}{2}$ excited state by an energy gap of $\frac{3}{2}J_{\rm ex}$. The pair of doublets is split into ground states and excited states by the DM interaction. (See also Refs. [27], [28].) The wave functions of the two Kramers doublets are symmetry determined, using the relevant spinor group C_3^*.

We consider the product basis of all possible spin states $\{|\gamma_1\gamma_2\gamma_3\rangle\}$, where γ_q is the spin projection of center q along the common Z-quantization axis, lying along the C_3-symmetry axis. For each center, $\gamma_q = \pm\frac{1}{2}$ (or α and β, respectively). To determine the behavior of $\{|\gamma_1\gamma_2\gamma_3\rangle\}$ under the rotational symmetry operations $\hat{C}_{3\pm}$, we must first understand the behavior of a single spin component, being either $|\alpha_q\rangle$ or $|\beta_q\rangle$.

The transformation properties of spin-$\frac{1}{2}$ eigenfunctions under a $\hat{C}_{3\pm}$ rotation read, where $\epsilon_\pm = e^{\pm 2\pi i/3}$,

$$\hat{C}_{3\pm}[|\alpha_q\rangle \quad |\beta_q\rangle] = [-\epsilon_\pm|\alpha_{q\pm1}\rangle \quad -\epsilon_\mp|\beta_{q\pm1}\rangle]. \qquad (3)$$

When $\hat{C}_{3+}$ ($\hat{C}_{3-}$) acts on the composite state $|\gamma_1\gamma_2\gamma_3\rangle$, the phase factors in Eq. (3) for the α and β components on different centers are compounded, whereas the spins are preserved but cyclically permuted as $|\gamma_3\gamma_1\gamma_2\rangle$ ($|\gamma_2\gamma_3\gamma_1\rangle$).

Consider the projectors $\hat{P}_\Gamma = \sum_O X_\Gamma^*(\hat{O})\hat{O}$ for the relevant spinor irreducible representations (irreps) $\Gamma = A_{3/2}$, $^1E_{1/2}$, $^2E_{1/2}$ with characters $X_\Gamma(\hat{O})$ under symmetry operations $\hat{O}$. We apply these projectors to states $|\beta\alpha\alpha\rangle$ and $|\alpha\beta\beta\rangle$. The rotation operators in the projectors transform $|\beta\alpha\alpha\rangle$ and $|\alpha\beta\beta\rangle$ into all the elements of $\{|\gamma_1\gamma_2\gamma_3\rangle\}$ with spin-projection $M_{\rm tot} = \pm\frac{1}{2}$. The phase factors ensure the elements are combined to form symmetry-adapted eigenstates of $\hat{H}_0$, Eq. (2).

Here, we only show the states in the ground exchange spin-frustrated manifold. Interestingly, these states can be classified not only by spin and by the irreps of the C_3^* spinor group, but also by the ±1 eigenvalues of the scalar spin chirality operator $\hat{\chi}$ [27]. We obtain the symmetry-adapted states as follows using the notation $|\Gamma, M_{\rm tot}, \chi\rangle$:

$$\begin{aligned}
\sqrt{3}|A_{3/2}, +1/2, +1\rangle &= |\beta\alpha\alpha\rangle + \epsilon_+|\alpha\beta\alpha\rangle + \epsilon_-|\alpha\alpha\beta\rangle,\\
\sqrt{3}|A_{3/2}, -1/2, -1\rangle &= |\alpha\beta\beta\rangle + \epsilon_-|\beta\alpha\beta\rangle + \epsilon_+|\beta\beta\alpha\rangle,\\
\sqrt{3}|\,^1E_{1/2}, +1/2, -1\rangle &= |\beta\alpha\alpha\rangle + \epsilon_-|\alpha\beta\alpha\rangle + \epsilon_+|\alpha\alpha\beta\rangle,\\
\sqrt{3}|\,^2E_{1/2}, -1/2, +1\rangle &= |\alpha\beta\beta\rangle + \epsilon_+|\beta\alpha\beta\rangle + \epsilon_-|\beta\beta\alpha\rangle. \qquad (4)
\end{aligned}$$

As alluded to above, the DM interaction splits the degeneracy of this manifold into two doublets, the energies being $+\frac{\sqrt{3}}{2}D_{\rm DM}$ for the $A_{3/2}$ states and $-\frac{\sqrt{3}}{2}D_{\rm DM}$ for the $E_{1/2}$ states. (See also Refs. [27,28].)

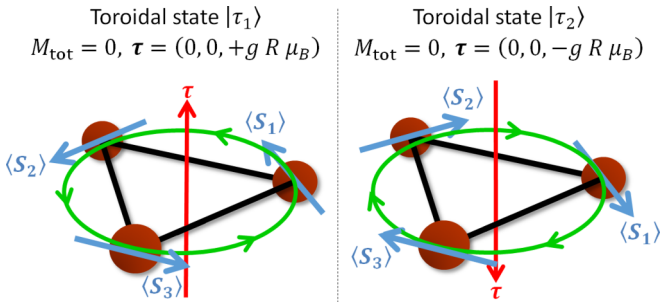

FIG. 1. The toroidal states $|\tau_1\rangle$ (left) and $|\tau_2\rangle$ (right) display mixed chirality, zero net dipole moment, and an in-plane circular magnetism (green). Expectation values for local spins $\langle \mathbf{S}_q\rangle$ are oriented tangentially with magnitudes of $\frac{1}{3}$ (blue). Toroidal moments $\boldsymbol{\tau}$ are perpendicular to the plane of the triangle (red).

We orient our triangle with one vertex on the X axis at $X = R > 0$, so the three atoms' position vectors form angles θ_q with the X axis: $\theta_1 = 0,\ \theta_2 = \frac{2\pi}{3},\ \theta_3 = -\frac{2\pi}{3}$. The Z component of the toroidal moment operator $\hat{\boldsymbol{\tau}}$, Eq. (1) then reads

$$\hat{\tau}_Z = -\frac{ig\mu_B R}{2}\sum_{q=1}^{3} e^{-i\theta_q}\hat{S}_{q+} - e^{i\theta_q}\hat{S}_{q-}, \tag{5}$$

where $\hat{S}_{q\pm} = \hat{S}_{qX} \pm i\hat{S}_{qY}$.

In the spin-frustrated manifold, the matrix representation of $\hat{\tau}_Z$ has nonzero elements *only* within the $A_{3/2}$ doublet and only between states of *opposite* spin chirality and *opposite* spin-projection $M_{\rm tot}$. Since the $A_{3/2}$ doublet is degenerate, the eigenstates of $\hat{\tau}_Z$ within the doublet form an equally valid representation of the doublet [33]. The eigenstates are termed $|\tau_1\rangle$ and $|\tau_2\rangle$ and have opposite toroidal moments, mixed chirality, and *zero magnetic moment*,

$$\sqrt{2}|\tau_{1,2}\rangle = \pm|A_{3/2},+1/2,+1\rangle + i|A_{3/2},-1/2,-1\rangle. \tag{6}$$

For both ground-states $|\tau_1\rangle$ and $|\tau_2\rangle$, the total spin expectation values are zero, see Eq. (7). The local spin-components' expectation values all lie on the XY plane and form toroidal vortex spin textures, shown in Fig. 1,

$$\langle S_{qX}\rangle = \mp\tfrac{1}{3}\sin\theta_q \quad \langle S_{qY}\rangle = \pm\tfrac{1}{3}\cos\theta_q \quad \langle S_{qZ}\rangle = 0. \tag{7}$$

Incidentally, we note here that $[\hat{\boldsymbol{\tau}}, \hat{\chi}] = \hat{\boldsymbol{\tau}}\hat{\chi} - \hat{\chi}\hat{\boldsymbol{\tau}} \neq 0$. We thus find it is not necessarily appropriate to refer to systems with a toroidal moment in their ground state as "chiral states" [8,34]. This is to be expected for our system since the pure toroidal states' local spin expectation values all lie on a plane, and all local spin operators on different centers commute with each other. Thus, each spin will be perpendicular to the cross product of its two neighbors, so the states should have zero spin chirality. On a side note, we report that the eigenstates of $\hat{\tau}_X$ and $\hat{\tau}_Y$ mix the $A_{3/2}$ and $E_{1/2}$ doublets, so toroidal moments in the X and Y directions are only possible when $D_{\rm DM} = 0$. These toroidal states have net magnetic moments in the Z direction as in Ref. [32] such that $\langle S_{qX}\rangle = \langle S_{qY}\rangle = 0$, $\langle S_{qZ}\rangle = \pm\frac{1}{2}$, and $\langle S_{\rm tot,Z}\rangle = \pm\frac{1}{2}$. The excited exchange $S_{\rm tot} = \frac{3}{2}$ states are completely nontoroidal.

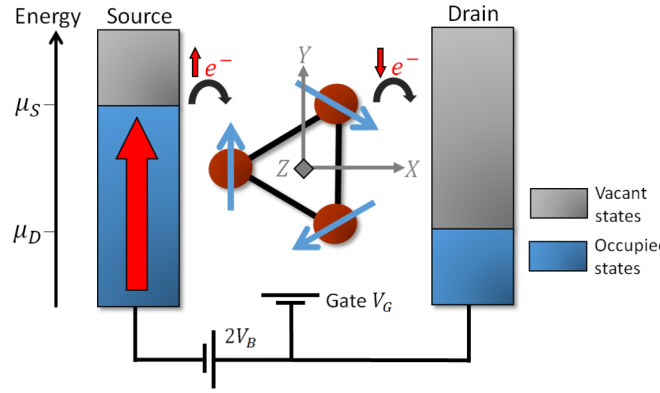

FIG. 2. Hypothetical spintronics device based on a toroidal nanomagnet. An external bias potential is applied to the source and drain leads so their Fermi levels are $\mu_S = +eV_B$ and $\mu_D = -eV_B$. An external gate potential $V_G = \frac{t-J_H}{2e}$ induces a resonance between the neutral and the singly charged ground states. The source lead is spin polarized; the drain lead is unpolarized. The device geometry is parametrized by the angles (ϕ, ζ, ω), corresponding to consecutive rotations about the (space-fixed) Z, Y, and X axes. The device is shown with the ideal geometry, $(\phi, \zeta, \omega) = (\frac{\pi}{3}, 0, 0)$ and the spin texture of uncharged state $|\tau_2\rangle$.

Next, we will address the question of how such ground states behave in a sequential tunneling molecular spintronics device.

III. THE SPIN TRANSPORT PROBLEM

A. The charge-transfer toroidal states

To explore the possibility of using these toroidal states in a frustrated molecular nanomagnet to achieve spin switching and the associated spin-transfer torque, we set up a spin transport model in the sequential tunneling regime. Our hypothetical spintronics device is depicted in Fig. 2. The source and drain leads are weakly hybridized with the spin triangle via the tunneling Hamiltonian [10,35–40],

$$\hat{H}_T = \sum_{q=1}^{3}\sum_{k}^{\text{first }BZ}\sum_{L}^{S,D}\sum_{\gamma}^{\uparrow,\downarrow}\beta_{qL}(\hat{a}^\dagger_{q\gamma}\hat{c}_{kL\gamma} + \hat{c}^\dagger_{kL\gamma}\hat{a}_{q\gamma}), \tag{8}$$

where $\hat{a}_{q\gamma}$ and $\hat{a}^\dagger_{q\gamma}$ annihilate and create, respectively, an electron on center q with spin γ; $\hat{c}_{kL\gamma}$ and $\hat{c}^\dagger_{kL\gamma}$ annihilate and create, respectively, an electron with wave-number k and spin γ on lead L; k varies in the first Brillouin zone characterizing a lead's electronic band structure; $L = S, D$ for the source and drain leads; $\gamma = \pm\frac{1}{2}$ is quantized along the source spin-polarization axis, which is defined to be parallel to the Y axis, see Fig. 2; β_{qL} is the coupling coefficient between center q and lead L and is modeled as being inversely proportional to the square of the distance from center q to lead L.

The analytical model for the device we are presenting here uses the ideal geometry shown in Fig. 2 with the triangle coplanar to the leads' spin-quantization axes. Later, we present the results of a more general model and explain why this geometry produces the strongest spin-transfer torque.

Since the leads are weakly hybridized with the triangle, we work under a model of sequential tunneling: An electron

can only tunnel from the source lead onto the triangle after the preceding electron has tunneled from the triangle to the drain. This is the Coulomb blockade regime in which doubly charged states of the triangle are assumed to be much higher in energy than the neutral- and singly charged states [10,35–40].

In our models, we use incoherent rate equations under the Born-Markov approximation. That is, we assume the leads are weakly coupled to the triangle, remain close to thermal equilibrium, and relax quickly, and we consider coherences between different states of the triangle to be negligible. The resulting master equation for the nonequilibrium populations of neutral states and singly charged states then becomes [10,35–40]

$$\frac{dP_j}{dt} = \sum_{i\neq j} P_i W_{i\to j} - P_j \sum_{i\neq j} W_{j\to i}, \tag{9}$$

where $W_{m\to n}$ is the charging/discharging rate from initial-state $|m\rangle$ to final-state $|n\rangle$.

Hence, we must now develop a model for the charge-transfer states for the singly reduced triangle. We assume the exchange coupling between the atomic centers to be the dominant energetic interaction and treat other interactions as perturbations. The first-order Hamiltonian $\hat{H}_1$ of the singly charged triangle then has three components [10,27,40,41],

$$\begin{aligned}
\hat{H}_{\rm DM} &= D_{\rm DM}\sum_{q=1}^{3}(\hat{\mathbf{S}}_q \times \hat{\mathbf{S}}_{q+1})_Z \\
\hat{H}_{\rm Hund} &= -J_H \sum_{q=1}^{3}\sum_{\gamma,\delta}^{\uparrow,\downarrow}[\hat{a}^\dagger_{q\gamma}\hat{a}_{q\delta}(\boldsymbol{\sigma})_{\gamma\delta}\cdot\hat{\mathbf{S}}_q] \\
\hat{H}_{\rm hop} &= t\sum_{q=1}^{3}\sum_{\gamma}^{\uparrow,\downarrow}(\hat{a}^\dagger_{q\gamma}\hat{a}_{q+1,\gamma} + \hat{a}^\dagger_{q+1,\gamma}\hat{a}_{q\gamma}).
\end{aligned} \tag{10}$$

These three components are as follows: (i) the DM interaction; (ii) a Hund's rule exchange-type interaction between the extra electron's spin and the local atomic spin arising from the uncharged states with coupling constant J_H; (iii) a hopping term describing intramolecular charge transfer of the extra electron between the atomic centers with hopping parameter t. The three Pauli matrices are collected in the vector of matrices $\boldsymbol{\sigma}$. The subscripts in $(\boldsymbol{\sigma})_{\gamma\delta}$ denote the row and column, respectively, of the elements to be used in the dot product with $\hat{\mathbf{S}}_q$.

We solve the DM and Hund interactions simultaneously under the limit of strong Heisenberg exchange and treat the hopping term as a further perturbation. That is, our solution for the charge-transfer states will apply to the regime: $-J_{\rm ex} \gg |D_{\rm DM}|,\ |J_H| \gg |t|$.

We describe the charge-transfer states using a basis of three localized atomic orbitals, denoted as $|q\gamma\rangle$ for the extra electron being on center q with spin γ initially quantized along the C_3 axis. The ground-state manifold from Heisenberg exchange coupling produces two toroidal and two nontoroidal uncharged states, see Sec. II. The direct product basis of these four uncharged states, three orbitals and two electron spins, yields a 24-dimensional Hilbert space for the charged system: $|\tau_i\rangle \otimes |q\gamma\rangle = |\tau_i; q\gamma\rangle$, where $i = 1$–4; $q = 1$–3; $\gamma = \pm\frac{1}{2}$; $|\,^1E_{1/2}, +\frac{1}{2}, -1\rangle \equiv |\tau_3\rangle$; $|\,^2E_{1/2}, -\frac{1}{2}, +1\rangle \equiv |\tau_4\rangle$.

First, we consider the DM interaction. From Eq. (10), we see that $\hat{H}_{\rm DM}$ is not affected by the extra electron. Because the product basis elements $|\tau_i; q\gamma\rangle$ form an orthonormal set, we then have

$$\langle\tau_j; q'\gamma'|\hat{H}_{\rm DM}|\tau_i; q\gamma\rangle = \xi_i\delta_{ij}\delta_{qq'}\delta_{\gamma\gamma'}, \tag{11}$$

where δ_{ij} is the Kronecker δ and the DM energies are $\xi_1 = \xi_2 = +\frac{\sqrt{3}}{2}D_{\rm DM}$ and $\xi_3 = \xi_4 = -\frac{\sqrt{3}}{2}D_{\rm DM}$. That is, the matrix representation $\mathbb{H}_{\rm DM}$ of the DM interaction is diagonal in the product basis.

Second, we consider the Hund interaction. In Eq. (10), $\hat{H}_{\rm Hund}$ does not couple states with the extra electron on different atomic centers. That is, $\langle\tau_j; q'\gamma'|\hat{H}_{\rm Hund}|\tau_i; q\gamma\rangle = 0$ if $q \neq q'$. Therefore, the matrix representation $\mathbb{H}_{\rm Hund}$ in the direct product basis $\{|\tau_i; q\gamma\rangle\}$ will be block diagonal, partitioned into three 8×8 problems. Each block will correspond to the eight basis elements possible for each center (four possible spin textures, two possible spins for the extra electron),

$$\hat{H}_{\rm Hund} \doteq \mathbb{H}_{\rm Hund} = -J_H\sum_{q=1}^{3}\sum_{\lambda}^{XYZ}\sigma_{q\lambda}\otimes\mathbb{T}_{q\lambda}, \tag{12}$$

where the matrices $\mathbb{T}_{q\lambda}$ are the representations of $\hat{\mathbf{S}}_q$ in the uncharged basis $\{|\tau_i\rangle\}$. The elements of $\mathbb{T}_{q\lambda}$ are $T_{ij,q\lambda} = \langle\tau_i|\hat{S}_{q\lambda}|\tau_j\rangle$, evaluated as matrix multiplications between the representations of $\langle\tau_i|$, $\hat{S}_{q\lambda}$, and $|\tau_j\rangle$ in the old product basis: $\{|\gamma_1\gamma_2\gamma_3\rangle\} = \{|\alpha\alpha\alpha\rangle,\ |\alpha\alpha\beta\rangle,\ |\alpha\beta\alpha\rangle,|\alpha\beta\beta\rangle,|\beta\alpha\alpha\rangle,|\beta\alpha\beta\rangle,|\beta\beta\alpha\rangle,|\beta\beta\beta\rangle\}$. The representations of $\hat{S}_{q\lambda}$ are built by taking the Kronecker products of the Pauli matrices and the 2×2 unit matrix in the appropriate order for site q: $\hat{S}_{1\lambda} \doteq \hbar\sigma_\lambda/2\otimes\mathbf{1}\otimes\mathbf{1}$, $\hat{S}_{2\lambda} \doteq \mathbf{1}\otimes\hbar\sigma_\lambda/2\otimes\mathbf{1}$, $\hat{S}_{3\lambda} \doteq \mathbf{1}\otimes\mathbf{1}\otimes\hbar\sigma_\lambda/2$.

We diagonalize the matrix $\mathbb{H}_{\rm DM} + \mathbb{H}_{\rm Hund}$ to obtain 24 eigenstates with energies,

$$\begin{aligned}
E_1 = E_2 = E_3 &= \frac{\sqrt{3}D_{\rm DM} - J_H}{2}, \\
E_4 = \cdots = E_9 &= \frac{-J_H - \sqrt{27D_{\rm DM}^2 + 4J_H^2}}{6}, \\
E_{10} = E_{11} = E_{12} &= \frac{-\sqrt{3}D_{\rm DM} - J_H}{2}, \\
E_{13} = E_{14} = E_{15} &= \frac{5J_H - \sqrt{27D_{\rm DM}^2 + 16J_H^2}}{6}, \\
E_{16} = \cdots = E_{21} &= \frac{-J_H + \sqrt{27D_{\rm DM}^2 + 4J_H^2}}{6}, \\
E_{22} = E_{23} = E_{24} &= \frac{5J_H + \sqrt{27D_{\rm DM}^2 + 16J_H^2}}{6}.
\end{aligned} \tag{13}$$

We want to study the spin transport properties of toroidal states and hence choose $D_{\rm DM} < 0$. For both cases $J_H > 0$ and $J_H < 0$, we find triply degenerate ground states which are always the ground states when $D_{\rm DM} < 0$, regardless of the ratio $|J_H|{:}|D_{\rm DM}|$ [42]. Without loss of generality, we discuss the case $J_H > 0$. That is, we assume ferromagnetic coupling

between the local atomic spins and the extra electron's spin, which is the physically most likely situation.

When $D_{\rm DM} < 0$ and $J_H > 0$, the extra electron aligns its spin along the toroidal spin textures produced by $|\tau_1\rangle$ and $|\tau_2\rangle$. So, to simplify the expressions for the ground states, we quantize our basis for the extra electron not along the C_3 axis, but rather along the tangential vectors to each atomic center. (The tangential vectors are equivalent to the directions of the local spin expectation values in $|\tau_1\rangle$, shown in Fig. 1.) The new noncollinear basis is termed $\{|\tau_i;\gamma q\rangle\}$, where $\uparrow q$ and $\downarrow q$ denote that the extra electron is located on center q, and the electron's spin is parallel or antiparallel to the local tangential axis on center q, respectively. Explicitly, we have

$$\begin{aligned}|\uparrow q\rangle &= 2^{-1/2}[e^{-i(\theta_q/2+\pi/4)}|\alpha_q\rangle + e^{i(\theta_q/2+\pi/4)}|\beta_q\rangle],\\ |\downarrow q\rangle &= 2^{-1/2}[-e^{-i(\theta_q/2+\pi/4)}|\alpha_q\rangle + e^{i(\theta_q/2+\pi/4)}|\beta_q\rangle].\end{aligned} \tag{14}$$

The expressions for the charge-transfer ground states when $D_{\rm DM} < 0$ and $J_H > 0$ then become for $q = 1$–3,

$$|\Psi_q\rangle = 2^{-1/2}(|\tau_1;\uparrow q\rangle - |\tau_2;\downarrow q\rangle). \tag{15}$$

We now allow the extra electron to be weakly delocalized across the three atomic centers. Assuming $\hat{H}_{\rm hop}$ represents the smallest energy scale, we reiterate perturbation theory to investigate the splitting of the charge-transfer ground states in Eq. (15). Since $\hat{H}_{\rm hop}$ is totally symmetric, its matrix representation will be block diagonal in a basis of symmetry-adapted functions, see Eq. (10). The symmetry group of the reduced triangle is still C_3^*, but now there is an even number of electrons. So, we require the projectors of the vector irreps A, ${}^1E$, and ${}^2E$ instead of the spinor irreps used in Sec. II.

Combining Eqs. (3) and (14), we find $\hat{C}_{3+}|\gamma 1\rangle = |\gamma 2\rangle$ and $\hat{C}_{3-}|\gamma 1\rangle = |\gamma 3\rangle$. By writing $|\tau_1\rangle$ and $|\tau_2\rangle$ in the old basis $\{|\gamma_1\gamma_2\gamma_3\rangle\}$, we find $\hat{C}_{3\pm}|\tau_{1,2}\rangle = -|\tau_{1,2}\rangle$. As such, applying the projectors of A, ${}^1E$, and ${}^2E$ to a charge-transfer state, such as $|\Psi_1\rangle$, produces the symmetry-adapted states below

$$\begin{aligned}|A\rangle &= 3^{-(1/2)}(|\Psi_1\rangle - |\Psi_2\rangle - |\Psi_3\rangle),\\ |E_{1,2}\rangle &= 3^{-(1/2)}(|\Psi_1\rangle - \epsilon_{\pm}|\Psi_2\rangle - \epsilon_{\mp}|\Psi_3\rangle).\end{aligned} \tag{16}$$

From Eqs. (10), (14), and (17), we find that $|A\rangle$, $|E_1\rangle$, and $|E_2\rangle$ are eigenstates of $\hat{H}_{\rm hop}$,

$$\hat{H}_{\rm hop}|E_{1,2}\rangle = \frac{t}{2}|E_{1,2}\rangle, \quad \hat{H}_{\rm hop}|A\rangle = -t|A\rangle. \tag{17}$$

At temperatures of $k_BT \ll |t|$, we can select only the ground state(s) among $|A\rangle$, $|E_1\rangle$, and $|E_2\rangle$. Since typically $t < 0$, $|E_1\rangle$, and $|E_2\rangle$ are the ground states of the charge-transfer system, see Eq. (17). In the next section, we will use the ground-states $|\tau_{1,2}\rangle$ and $|E_{1,2}\rangle$ to develop an analytical spin transport model working under the limit, $-J_{\rm ex} \gg -D_{\rm DM}$, $J_H \gg -t \gg k_BT > 0$.

B. Spin switching and population splitting

Assuming weak coupling between the triangle and the leads, we use the Fermi golden rule to compute the rates of all tunneling processes through the triangle [10,35–37]. Assuming that the lead-molecule coupling matrix elements (β_{qL}) and the density of spin states in the leads ($\rho_{L\gamma}$) are approximately energy independent around the Fermi energies of the leads, in evaluating the charging/discharging rates between a charged state $|E_j\rangle$ and a triangle-lead entangled state $|\tau_i;L\gamma\rangle$ generated by the molecule-lead Hamiltonian Eq. (8), the sum over k can be turned into an energy integral, resulting in [40]

$$\begin{aligned}W^{L\gamma}_{\tau_i\to E_j} &= \frac{2\pi\rho_{L\gamma}}{\hbar}\left|\langle E_j|\sum_{q=1}^{3}\beta_{qL}a^{\dagger}_{q\gamma}|\tau_i\rangle\right|^2 F_L(\Delta_{E,\tau}),\\ W^{L\gamma}_{E_j\to\tau_i} &= \frac{2\pi\rho_{L\gamma}}{\hbar}\left|\langle\tau_i|\sum_{q=1}^{3}\beta_{qL}a_{q\gamma}|E_j\rangle\right|^2 [1 - F_L(\Delta_{E,\tau})],\end{aligned} \tag{18}$$

where $F_L(\xi) = [1+\exp(\frac{\xi-\mu_L}{k_BT})]^{-1}$ and $\Delta_{E,\tau}$ is the energy gap between the charge-transfer ground-state $|E_{1,2}\rangle$ and the toroidal ground state of the uncharged triangle $|\tau_{1,2}\rangle$. When the conduction window is small (i.e., at low temperature and weak bias voltage), an external gate voltage V_G is applied so that $\Delta_{E,\tau} \to 0$. From Eq. (17), we see that $|E_1\rangle$ and $|E_2\rangle$ differ only by a phase factor in their components hence $W^{L\gamma}_{\tau_i\to E_1} = W^{L\gamma}_{\tau_i\to E_2}$ and $W^{L\gamma}_{E_1\to\tau_i} = W^{L\gamma}_{E_2\to\tau_i}$.

In an ideal device, the source would be fully spin-up polarized, and the drain would be unpolarized: $\rho_{S\downarrow} = 0$, $\rho_{D\uparrow} = \rho_{D\downarrow} = \frac{1}{2}\rho_{S\uparrow}$. So, for the geometry $(\phi,\zeta,\omega) = (\frac{\pi}{3},0,0)$ with coupling coefficients $\{\beta_{1S},\beta_{2S},\beta_{3S},\beta_{1D},\beta_{2D},\beta_{3D}\} = \{0,\beta_S,0,\beta_D,0,\beta_D\}$, the local spin on center two in $|\tau_2\rangle$ is parallel to the source's spin polarization, see Fig. 2.

This alignment causes charging from the source lead to be performed exclusively to $|\tau_2\rangle$ when J_H is ferromagnetic. However, when discharging to the drain, it is possible to repopulate both $|\tau_1\rangle$ and $|\tau_2\rangle$. So, as electrons are driven by the bias voltage from the source to the drain, the device gradually transfers the nonequilibrium population from $|\tau_2\rangle$ to $|\tau_1\rangle$. Conversely, when electrons flow against the bias voltage, $|\tau_2\rangle$ is repopulated. Thus, the populations of $|\tau_1\rangle$ and $|\tau_2\rangle$ are split by the bias voltage, see Fig. 3. Next, we will quantify this effect.

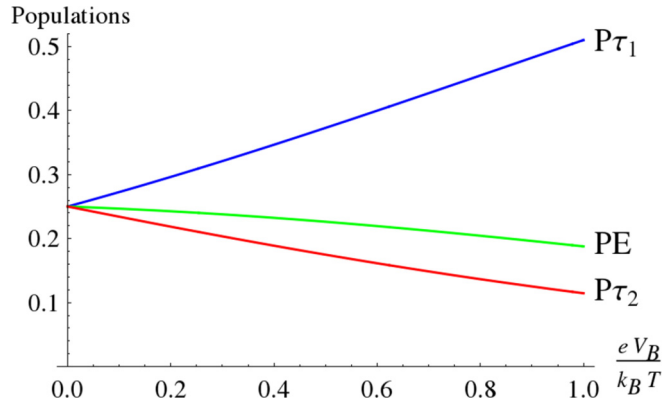

FIG. 3. Nonequilibrium populations vs eV_B/k_BT, showing $P\tau_1$, $P\tau_2$, and $PE_1 = PE_2 \equiv PE$, see Eq. (19). The bias voltage V_B splits the populations of the ground toroidal states $|\tau_1\rangle$ and $|\tau_2\rangle$ as spin transport is performed via $|\tau_2\rangle$ and $|E_{1,2}\rangle$. Analytical calculation in the four-state model, ideal geometry, $\beta_S/\beta_D = 2$, $J_H > 0$.

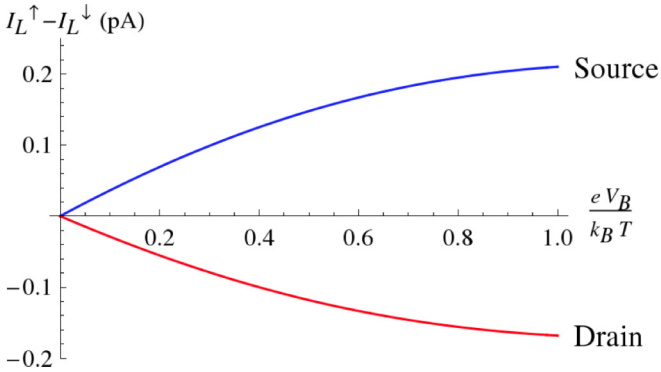

FIG. 4. Source and drain spin currents vs eV_B/k_BT. The spin current's polarization is partially reversed by the toroidal spin texture of the triangle, giving $-(I_D^{\uparrow} - I_D^{\downarrow})/(I_S^{\uparrow} - I_S^{\downarrow}) = 0.8$, see Eq. (21). Analytical calculation in the four-state model, ideal geometry, $\beta_S/\beta_D = 2$, $\rho_{S\uparrow} = 1$ cm.

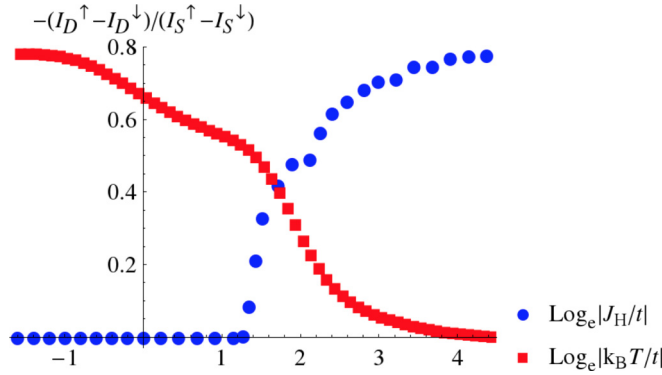

FIG. 5. [(a) blue circles] Spin-switching vs $\mathrm{Log}_e|J_H/t|$, varying t for fixed $J_H = 10\ \mathrm{cm}^{-1}$, $T = 50$ mK. The ideal regime for strong switching is $|J_H/t| \gg 1$. [(b) red squares] Spin switching vs $\mathrm{Log}_e|k_BT/t|$, varying T for fixed $J_H = 10\ \mathrm{cm}^{-1}$, $t = -0.1\ \mathrm{cm}^{-1}$. The ideal regime for strong switching is $-t \gg k_BT$. Both calculations performed with the 28-state numerical program, ideal geometry, $\beta_S/\beta_D = 2$, $eV_B = 0.001\ \mathrm{cm}^{-1}$, $J_H/D_{\mathrm{DM}} = -\sqrt{3}$.

The master equation Eq. (9) can be solved analytically under the steady-state approximation to give

$$
\begin{aligned}
P\tau_1 &= \eta\left[4\beta_S^2 \exp\left(\frac{eV_B}{k_BT}\right) + 5\beta_D^2\right],\\
P\tau_2 &= \eta\left[4\beta_S^2 \exp\left(\frac{-eV_B}{k_BT}\right) + 5\beta_D^2\right],\\
PE_1 &= PE_2 \equiv PE = \eta\left[4\beta_S^2 + 5\beta_D^2 \exp\left(\frac{-eV_B}{k_BT}\right)\right],
\end{aligned}
\tag{19}
$$

where η is a normalization constant.

Notice that as V_B/T increases, $P\tau_1$ approaches unity whereas $P\tau_2$ and PE approach zero, see Fig. 3. Therefore, by controlling V_B/T, one might be able to control the splitting between $P\tau_1$ and $P\tau_2$ and initialize a toroidal qubit as $|\tau_1\rangle$. To initialize a qubit as $|\tau_2\rangle$, one would only need to reverse the direction of the bias voltage.

This population splitting can be viewed as evidence for spin-transfer torque with rotating electron spins altering the triangle's spin texture. To quantify the strength of the spin-transfer torque, we calculate the extent of switching of the polarization of the spin currents through the source and drain leads. For the ideal geometry $(\phi, \zeta, \omega) = (\frac{\pi}{3}, 0, 0)$, the spin currents are (see also Fig. 4) as follows:

$$
\begin{aligned}
I_S^{\uparrow} - I_S^{\downarrow} &= \frac{10\pi e\beta_S^2\beta_D^2\eta\rho_{S\uparrow}}{3\hbar}\left[1 - \exp\left(\frac{-eV_B}{k_BT}\right)\right],\\
I_D^{\uparrow} - I_D^{\downarrow} &= -\frac{4}{5}(I_S^{\uparrow} - I_S^{\downarrow}).
\end{aligned}
\tag{20}
$$

This is a large spin-switching effect, which is independent of V_B, T, β_S, and β_D as long as these parameters are small enough for our approximations to be valid.

Next, we wrote a computer program to calculate the nonequilibrium populations of all 28 states and from them determine the spin current and the strength of spin switching: $-(I_D^{\uparrow} - I_D^{\downarrow})/(I_S^{\uparrow} - I_S^{\downarrow})$. The program has been used to diagonalize the charged triangle's first-order Hamiltonian without perturbation theory and thus to confirm the findings of the analytical model and to explore further details concerning the device's properties, including a study of its spin-switching performance as a function of its spatial orientation with respect to the spin-polarized source lead.

For example, we find that our device produces stronger spin switching when $|J_H/t| \gg 1$ as in Fig. 5(a) because: (i) If the intramolecular charge transfer can compete with the Hund coupling to local spins, the extra electron may tunnel to the drain lead before its spin is altered; (ii) the Hund coupling produces a spin torque on the tunneling electron as it crosses the triangle. However, if the electron is strongly delocalized and couples to multiple centers simultaneously, the spin torque will be diminished.

Our device also performs best when $-t \gg k_BT$, so $|E_1\rangle$ and $|E_1\rangle$ are populated rather than $|A\rangle$ as in Fig. 5(b). This is because the tunneling electron can discharge to the drain via centers one *and* three when $(\phi, \zeta, \omega) = (\frac{\pi}{3}, 0, 0)$, see Fig. 2. Discharging from $|E_{1,2}\rangle$ to $|\tau_2\rangle$, these two pathways interfere favorably, but when discharging from $|A\rangle$ to $|\tau_2\rangle$, the $|\Psi_3\rangle$ component's phase in Eq. (17) causes the pathways to interfere unfavorably. Thus, when $-t \gg k_BT$ and $(\phi, \zeta, \omega) = (\frac{\pi}{3}, 0, 0)$, the strength of switching decreases by 37% if the drain only couples to one center rather than to both centers equally.

The geometry $(\phi, \zeta, \omega) = (\frac{\pi}{3}, 0, 0)$ in Fig. 2 is ideal for three reasons. First, the selectivity for $|\tau_1\rangle$ or $|\tau_2\rangle$ upon charging from the source is strongest when there is only one center coupled to the source, and its spin is aligned with the source's spin polarization. This requires $\sin\omega = 0$, small $|\sin\zeta|$, and $\phi = \frac{\pi}{3}, \pi, \frac{5\pi}{3}$, see Fig. 6. When the alignment is imperfect, the charging selectivity is worsened further by increasing V_B/T and/or β_S/β_D.

Second, it is desirable that the center(s) coupled to the drain have spin(s) aligned vertically along the drain's spin-quantization axis, e.g., $\sin\omega = 0$, $\phi = 0, \frac{2\pi}{3}, \frac{4\pi}{3}$. However, we found that charging selectivity is more important. Choosing $\sin\omega = 0$ and $\phi = \frac{\pi}{3}, \pi, \frac{5\pi}{3}$ is the best compromise between charging selectivity and having a vertical spin coupled to the drain, see Figs. 6(a) and 6(b).

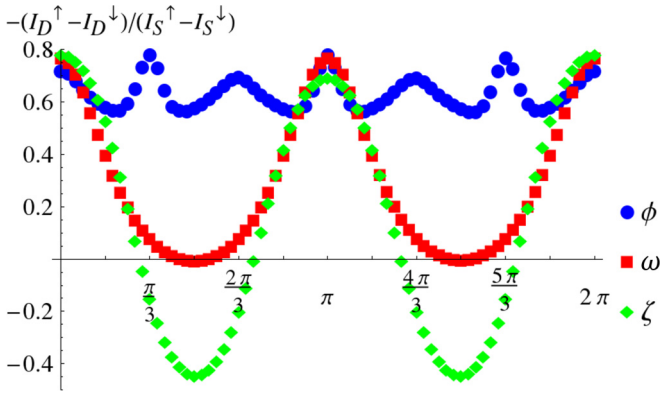

FIG. 6. [(a) blue circles] Spin switching vs ϕ for fixed $\zeta = \omega = 0$, $\beta_{qS} = \{\max[0, \cos(\phi + \theta_q + \pi)]\}^2$ cm^{-1}, $\beta_{qD} = \{\max[0, \cos(\phi + \theta_q)]\}^2$ cm^{-1}. There are local maxima when an atomic center's tangential axis is aligned with a lead's spin-quantization axis. [(b) red squares] Spin switching vs ω for fixed $\phi = \frac{\pi}{3}$, $\zeta = 0$, $(\beta_{1S}, \beta_{2S}, \beta_{3S}, \beta_{1D}, \beta_{2D}, \beta_{3D}) = (0, 1, 0, \frac{3}{4}, 0, \frac{3}{4})$ cm^{-1}. There are minima when the triangle's plane is perpendicular to the leads' spin-quantization axes. [(c) green diamonds] Spin switching vs ζ for fixed $\phi = \frac{\pi}{3}$, $\omega = 0$, $\beta_{1S} = \beta_{3S} = \frac{1}{4}\beta_{2D} = \frac{1}{4}\sin^2(\frac{\zeta}{2})$ cm^{-1}, $\beta_{1D} = \beta_{3D} = \frac{1}{4}\beta_{2S} = \frac{1}{4}\cos^2(\frac{\zeta}{2})$ cm^{-1}. There are minima when each lead couples to all three centers equally. Each calculation performed with the 28-state numerical program $eV_B = 0.001$ cm^{-1}, $J_H/D_{\rm DM} = -\sqrt{3}$, $J_H/t = -100$, $T = 10$ mK.

Third, a small $|\sin\zeta|$ ensures each center is only coupled to one lead. This means the tunneling electron must cross the triangle's toroidal spin texture before discharging from a particular center rather than discharging immediately without its spin being altered, see Fig. 6(c). In this geometry, the bias voltage would produce an electric field parallel to the plane of the triangle, which would weaken the spin switching by mixing the states with A and E symmetries. However, this effect is minimized when $-D_{\rm DM} \gg -t \gg eV_B$, so a small $|\sin\zeta|$ is still desirable.

An interesting feature of Fig. 6 is that in-plane rotations do not greatly affect the extent of spin switching, but out-of-plane rotations do. Integrating over $\phi \in [0, 2\pi)$ in Fig. 6(a) gives an average spin switching of 0.638, but in Figs. 6(b) and 6(c), the averages over ω and ζ are 0.335 and 0.151, respectively. Thus, optimal spin switching and optimal spin-transfer torque can be achieved by ensuring that the triangle's plane is parallel to the leads' spin-quantization axes, whereas some disorder pertaining to in-plane rotations of the triangular toroidal device is not expected to greatly affect our conclusions.

IV. SUMMARY

A triangular ring with on-site spins $S_q = \frac{1}{2}$, strong antiferromagnetic exchange coupling, and weak spin-orbit coupling can be prepared in a noncollinear ground spin state with a zero magnetic moment and a nonzero toroidal moment $\boldsymbol{\tau} = (0, 0, \pm gR\mu_B)$. These toroidal states are prepared in the ground Kramers doublet from weak Dzyaloshinskii-Moriya antiferromagnetic exchange coupling as coherent combinations of states with $A_{3/2}$ symmetry, opposite spin chirality, and opposite spin projection. In the singly charged triangle's ground states, a weakly delocalized extra electron aligns its spin along the triangle's toroidal spin textures.

The toroidal states of the spin triangle and their charge-transfer derivatives were used to construct a model for spin transport through a three-terminal device in the sequential tunneling regime. Under optimal conditions, the device is found to split the nonequilibrium populations of the ground toroidal states stabilizing a nonzero toroidal polarization in the molecular device. This also results in the partial switching of the polarization of a spin current passing through the triangle: $-(I_D^{\uparrow} - I_D^{\downarrow})/(I_S^{\uparrow} - I_S^{\downarrow}) \to 0.8$. We predict that such a device would work best with a planar geometry and system parameters: $-J_{\rm ex} \gg -D_{\rm DM}$, $|J_H| \gg -t \gg k_BT, |eV_B|$, $|\beta_S|$, $|\beta_D| > 0$.

In conclusion, our results suggest that, by controlling the bias voltage in a device built according to our specifications, it will be possible to selectively control the toroidal polarization of the molecular device, which can be monitored by the amount of spin switching measured between an in-plane spin-polarized source electrode and, e.g., a drain electrode having opposite spin polarization.

ACKNOWLEDGMENTS

A.S. acknowledges financial support from the Australian Research Council, through a Discovery Grant, project ID: DP150103254. J.M.C. acknowledges financial support from an Australian Government Research Training Program Scholarship. The authors thank Professor M. Affronte, Dr. A. Candini, and K. Hymas for useful discussions.

[1] V. L. Ginzburg, A. A. Gorbatsevich, Y. V. Kopayev, and B. A. Volkov, Solid State Commun. **50**, 339 (1984).
[2] B. B. V. Aken, J.-P. Rivera, H. Schmid, and M. Fiebig, Nature (London) **449**, 702 (2007).
[3] N. A. Spaldin, M. Fiebig, and M. Mostovoy, J. Phys.: Condens. Matter **20**, 434203 (2008).
[4] F. Faglioni, A. Ligabue, S. Pelloni, A. Soncini, and P. Lazzeretti, Chem. Phys. **304**, 289 (2004).
[5] D. I. Khomskii, *Transition Metal Compounds* (Cambridge University Press, Cambridge, U.K., 2014).
[6] A. Soncini and L. F. Chibotaru, Phys. Rev. B **77**, 220406(R) (2008).
[7] L. F. Chibotaru, L. Ungur, and A. Soncini, Angew. Chem., Int. Ed. **47**, 4126 (2008).
[8] J. Luzon, K. Bernot, I. J. Hewitt, C. E. Anson, A. K. Powell, and R. Sessoli, Phys. Rev. Lett. **100**, 247205 (2008).
[9] J. Tang, I. J. Hewitt, N. T. Madhu, G. Chastanet, W. Wernsdorfer, C. E. Anson, C. Benelli, R. Sessoli, and A. K. Powell, Angew. Chem., Int. Ed. **45**, 1729 (2006).
[10] A. Soncini and L. F. Chibotaru, Phys. Rev. B **81**, 132403 (2010).

[11] D. I. Plokhov, A. I. Popov, and A. K. Zvezdin, Phys. Rev. B **84**, 224436 (2011).
[12] D. I. Plokhov, A. I. Popov, and A. K. Zvezdin, Phys. Rev. B **83**, 184415 (2011).
[13] I. J. Hewitt, J. Tang, N. T. Madhu, C. E. Anson, Y. Lan, J. Luzon, M. Etiennne, R. Sessoli, and A. K. Powell, Angew. Chem., Int. Ed. **49**, 6352 (2010).
[14] S.-Y. Lin, W. Wernsdorfer, L. Ungur, A. K. Powell, Y.-N. Guo, J. Tang, L. Zhao, L. F. Chibotaru, and H.-J. Zhang, Angew. Chem., Int. Ed. **51**, 12767 (2012).
[15] K. R. Vignesh, A. Soncini, S. K. Langley, W. Wernsdorfer, K. S. Murray, and G. Rajaraman, Nat. Commun. **8**, 1023 (2017) .
[16] G. Novitchi, G. Pilet, L. Ungur, V. V. Moshchalkov, W. Wernsdorfer, L. F. Chibotaru, D. Luneau, and A. K. Powell, Chem. Sci. **3**, 1169 (2012).
[17] L. Ungur, S.-Y. Lin, J. Tang, and L. Chibotaru, Chem. Soc. Rev. **43**, 6894 (2014).
[18] S. Krause, L. Berbil-Bautista, G. Herzog, M. Bode, and R. Wiesendanger, Science **317**, 1537 (2007).
[19] R. E. P. Winpenny, Angew. Chem., Int. Ed. **47**, 7992 (2008).
[20] A. S. Zyazin, H. S. J. van der Zant, M. R. Wegewijs, and A. Cornia, Synth. Met. **161**, 591 (2011).
[21] A. Candini, S. Klyatskaya, M. Ruben, W. Wernsdorfer, and M. Affronte, Nano Lett. **11**, 2634 (2011).
[22] M. Urdampilleta, S. Klyatskaya, J.-P. Cleuziou, M. Ruben, and W. Wernsdorfer, Nat. Mater. **10**, 502 (2011).
[23] R. Vincent, S. Klyatskaya, M. Ruben, W. Wernsdorfer, and F. Balestro, Nature (London) **488**, 357 (2012).
[24] S. Thiele, F. Balestro, R. Ballou, S. Klyatskaya, M. Ruben, and W. Wernsdorfer, Science **344**, 1135 (2014).
[25] S. Lumetti, A. Candini, C. Godfrin, F. Balestro, W. Wernsdorfer, S. Klyatskaya, M. Ruben, and M. Affronte, Dalton Trans. **45**, 16570 (2016).
[26] D. Gatteschi, R. Sessoli, and J. Villain, *Molecular Nanomagnets* (Oxford University Press, Oxford, U.K., 2006).
[27] M. Trif, F. Troiani, D. Stepanenko, and D. Loss, Phys. Rev. Lett. **101**, 217201 (2008).
[28] M. F. Islam, J. F. Nossa, C. M. Canali, and M. Pederson, Phys. Rev. B **82**, 155446 (2010).
[29] J. F. Nossa, M. F. Islam, C. M. Canali, and M. R. Pederson, Phys. Rev. B **85**, 085427 (2012).
[30] K.-Y. Choi, Z. Wang, H. Nojiri, J. van Tol, P. Kumar, P. Lemmens, B. S. Bassil, U. Kortz, and N. S. Dalal, Phys. Rev. Lett. **108**, 067206 (2012).
[31] S. Bertaina, S. Gambarelli, T. Mitra, B. Tsukerblat, A. Müller, and B. Barbara, Nature (London) **453**, 203 (2008).
[32] A. K. Zvezdin, V. V. Kostyuchenko, A. I. Popov, A. F. Popkov, and A. Ceulemans, Phys. Rev. B **80**, 172404 (2009).
[33] In practice, to prepare the $A_{3/2}$ Kramers doublet in a toroidal configuration, a splitting field gradient $\nabla \times \mathbf{B}$ should be applied along the Z axis [4] or, equivalently, a current should flow along the Z direction [12].
[34] S. Carretta, G. Amoretti, P. Santini, V. Mougel, M. Mazzanti, S. Gambarelli, E. Colineau, and R. Caciuffo, J. Phys.: Condens. Matter **25**, 486001 (2013).
[35] F. Delgado, J. J. Palacios, and J. Fernàndez-Rossier, Phys. Rev. Lett. **104**, 026601 (2010).
[36] G.-H. Kim and T.-S. Kim, Phys. Rev. Lett. **92**, 137203 (2004).
[37] M. Misiorny and J. Barnaś, Phys. Status Solidi B **246**, 695 (2009).
[38] F. Elste and C. Timm, Phys. Rev. B **71**, 155403 (2005).
[39] G. González and M. N. Leuenberger, Phys. Rev. Lett. **98**, 256804 (2007).
[40] A. Soncini, T. Mallah, and L. F. Chibotaru, J. Am. Chem. Soc. **132**, 8106 (2010).
[41] B. Georgeot and F. Mila, Phys. Rev. Lett. **104**, 200502 (2010).
[42] If $J_H < 0$, ground energies in Eq. (13) are E_{13}, E_{14}, E_{15}.